IEEE Access
Multidisciplinary | Rapid Review | Open Access Journal

Received July 2, 2020, accepted July 10, 2020, date of publication July 17, 2020, date of current version July 29, 2020.

Digital Object Identifier 10.1109/ACCESS.2020.3010202

Code Division Multiple Access Wireless Power Transfer for Energy Sharing in Heterogenous Robot Swarms

AKSHAY SARIN, (Member, IEEE), AND AL-THADDEUS AVESTRUZ, (Member, IEEE)
Department of Electrical Engineering and Computer Science, University of Michigan at Ann Arbor, Ann Arbor, MI 48109, USA
Corresponding author: Akshay Sarin (akisarin@umich.edu)

ABSTRACT Energy is one of the key enablers for robotic swarms. The feasibility of heterogeneous swarms to perform complex missions depends upon the energy stored in the robot batteries. Allowing multiple access energy transfer (MAET) in robot swarms provides more flexibility to accomodate uncertain missions. In this paper, we present a MAET solution for heterogeneous swarms using code division multiple access wireless power transfer (CDMA-WPT). CDMA-WPT allows robots in heterogeneous swarms to exchange energy while in motion, allows faster charging rates by enabling multiple robots to exchange energy, is easily scalable, offers power flow selectivity to enable energy encryption, and does not require a centralized controller. The encoding scheme, power flow model, and code construction algorithm for a particular implementation of CDMA-WPT is presented. The proof of concept is verified using a hardware implementation for a heterogeneous swarm of four robots. Finally, the application of CDMA-WPT to a heterogeneous swarm with 30 robots is presented.

INDEX TERMS Code division multiple access, energy sharing, heterogeneous swarms, multiple access energy transfer, wireless power transfer, robot swarms, energy networks, resonant converters, distributed power, power networks, zero voltage switching.

I. INTRODUCTION

Stored energy is a fundamental resource for robotic swarms. The past few decades have seen tremendous growth in sensing, computation, and control technology leading to enormous development in the field of swarm robotics. However, the capabilities of these robotic swarms are ultimately limited by the battery capacity of each robot. The stored electrical energy in the robots is usually a hard constraint when optimizing the resources and the performance of robotic swarms. A key concept for swarm robotics is fostering collaborative actions among robots to accomplish complex missions [1]. This cooperation and coordination is especially important for heterogeneous robotic swarms to allow simpler, but more varied robots to complete complex missions [2]; the ability to complete these complex missions depends on the battery life of each robot. Estimating the energy requirements for each robot apriori is difficult and varies from mission to mission. This typically incurs overcapacity for each individual robot to contend with uncertainty, and thus obligates tradeoffs in other capabilities. If during a particular mission a robot runs out of energy, the mission will be unsuccessful. Hence, the feasibility of each mission depends on the ability of each robot to complete its assigned tasks with the limited energy stored in its battery. To overcome this limitation, there is a need to develop ad-hoc energy networks among robots to allow energy exchange and to envision energy as a collective resource for the entire swarm.

As an example, consider the swarmanoid robots described in [2] with a foot bot, hand bot, and eye bot. The footbot is primarily used for ground locomotion and carrying the handbot; the handbot is responsible for gripping and climbing and the eye bot is responsible for sensing of otherwise inaccessible areas. Each hand bot and foot bot is equipped with a battery pack having a total energy of 37 Wh. If a particular mission requires the handbot to climb horizontally 5 times, with each climbing activity requiring 9 Wh of energy, then the total energy required for the hand bots is 45 Wh. To complete this mission, we either require two hand bots or instead allow the foot bot to transfer energy to the hand bot. If the total

The associate editor coordinating the review of this manuscript and approving it for publication was Jiankang Zhang.

energy consumption of a foot bot during the mission is 20 Wh, then by transferring 10 Wh of energy from the foot bot to the hand bot, the mission can be completed without requiring additional robots or external recharging of the robots. Thus, energy sharing in robot swarms offers greater flexibility to complete missions.

Energy sharing is particularly important in contending with mission variability and uncertainty. To fully take advantage of energy sharing, robots should be capable of receiving and transmitting power as needed, thereby allowing bidirectional flow of energy.

There have been multiple ideas for recharging robots that have been presented in the literature. References [3] and [4] present the idea of recharging robots from fixed transmitting points in space. Although it is possible for these recharging solutions to have been wired, using galvanic conductors for recharging would have added mission constraints on the swarm. Thus, most of the solutions in the literature have focused on the wireless charging of robots. References [5] and [6] provide near-field inductive wireless charging solutions for the robotic swarms with the capability of recharging from fixed stations. However, traveling to a fixed point during a mission consumes both time and energy. Reference [7] presents the concept of using an autonomous robot for the recharging needs during a mission using *peer-to-peer (P2P)* power transfer. Not only does this approach require an additional robot, but recharging is slow because multiple robots have to take turns. Also, the robots are still required to travel to the transmitting robot to recharge. Thus, there is a need for moving away from fixed infrastructure recharging and P2P recharging to the concept of multiple access energy transfer (MAET) where multiple robots can share energy simultaneously. MAET allows robots to charge each other cooperatively, thus can enable faster recharging because multiple robots can power one robot. MAET helps create ad-hoc energy networks with different topologies including the mesh topology, star topology, and other hybrid topologies, offering a flexible platform for the robots to share energy. These ad-hoc energy networks allow the robots to remain in their formations as dictated by the mission while still allowing recharge, thereby providing more flexibility to contend with uncertainties.

The rapid growth of wireless power transfer (WPT) in recent times has led to the development of a number of solutions for multiple access in WPT. Some of the MAET solutions include single-input-multiple-output (SIMO) WPT systems [8], [9], multiple-input-single-output (MISO) systems [10], [11], and multiple-input-multiple-output systems (MIMO) [12], [13]. With multiple transmitters and receivers in the same electromagnetic space, there is unintended interference in the energy transfer. Prevailing multiple access solutions either compensate for the unintended interference by using control methods, using impedance compensation techniques, or avoiding interference by operating in different slots of time, frequency, or space. Although applications of these popular MAET WPT techniques can be applied to robotic swarms [14], their lack of scalability as well as lack of power flow selectivity makes them unsuitable for developing ad-hoc wireless charging networks for robotic swarms. Reference [15] provides algorithms, strategies, and techniques for wireless charging that specifically focus on wireless sensor nodes. Some of these techniques in [15], including the charge traversal decision for a mobile charger, recharge scheduling, and collaborative mobile charging using multiple chargers, can be promising for developing ad-hoc energy networks in robotic swarms. However, the strategies presented do not take advantage of the flexibility offered by MAET. To best use these ad-hoc energy networks, it is imperative to include the various possible energy exchange solutions in the hardware design and planning process of the robotic swarms [16].

The emergence of code division multiple access (CDMA) for WPT offers a catalyst for developing new ad-hoc wireless energy networks for heterogeneous robotic swarms. In [17], we presented the first application of CDMA for WPT using half sine voltage pulses encoded as ternary codes. The first demonstration of power exchange using ternary codes was presented in [18]. In [19], receiver topologies were presented for receiving maximum power from these ternary sequences. In [20], we presented the transceiver hardware for realizing CDMA-WPT. In this paper, we build on these previously introduced concepts in CDMA-WPT, towards approaches for ad-hoc wireless power networks for energy sharing in heterogeneous robotic swarms.

This paper presents a framework and technical details for a method to enable MAET in heterogeneous swarms. To the best of the authors' knowledge, this paper is the first attempt at enabling multiple access energy sharing in swarms with the promise of opening new avenues of research in the areas of energy networks and architectures, algorithms and strategies for swarm energy distribution, dynamic reconfiguration of energy, and using the energy sharing to the greatest advantage based on the mission.

II. MULTIPLE ACCESS ENERGY TRANSFER

To allow heterogeneous swarms to take the maximum advantage of MAET, energy transfer should have the following desirable characteristics:

1) **Power flow selectivity:** Behavioral control is a challenge for robotic swarms. Thus, the energy transfer mechanism should be capable of controlling the power flow to the selected robots and not be influenced by the other robots in the environment. The energy transfer requirement should not add behavioral constraints for electromagnetically isolating the robots that are sharing energy. The swarm might require protection from adversarial robots trying to steal or disrupt power, and hence it may be advantageous to encrypt the energy transfer [21].
2) **Scalability:** One of the important characteristics of robotic swarms is scalability [22]; thus, MAET should also easily scale to large swarms.

3) **Distributed control:** One of the main advantages in using robotic swarms is the ability to operate without the need for a centralized controller, thus MAET should be capable of decentralized operation [23].
4) **Bidirectional capability:** Every robot in the swarm must be capable of both sending and receiving energy as needed.
5) **Energy transfer while in motion:** The energy transfer mechanism must not restrict the free movement of the robots and should not interrupt their mission and tasks.
6) **Robustness:** Solutions should be robust to extreme conditions like high vibration and corrosive environments like seawater, among others.

A possible solution for developing MAET in robotic swarms is galvanically wired connections with conductive connectors. The conductive connections, however, restrict the free motion of the robots. Additionally, the mechanical connectors are prone to failure in harsh corrosive environments (underwater) or high vibration surroundings. The connectors are also prone to wear and have a limited life-cycle. This makes them unreliable and over time could result in unexpected electrical failures [24].

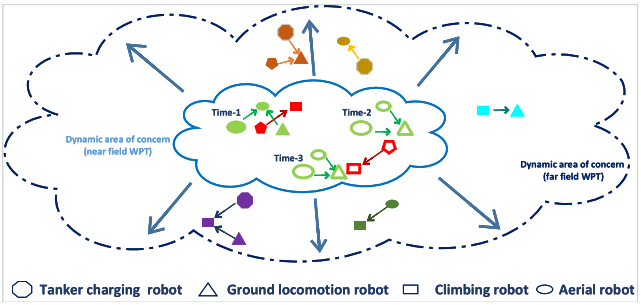

FIGURE 1. Robots in a heterogeneous swarm exchanging energy through WPT while performing a mission. The ad-hoc network provides the capability of dynamic reconfiguration of energy transfer at different times. The robots in the neighborhood of influence can both effect or affect power transfer. The neighborhood of influence may be bigger or smaller based on the type of WPT system employed.

WPT is a compelling solution for energy sharing in heterogeneous robotic swarms. Unlike conductive energy transfer, it does not restrict the movement of the robots and allows them to exchange energy without interrupting the mission as illustrated in Fig. 1. WPT does not employ mechanical connectors making it possible to perform energy exchange in underwater environments with hermetically sealed robots. WPT technology has grown rapidly in the past two decades with demonstrated applications for charging biomedical implants [25], electronic devices [26], and electric vehicles [27].

A well-known solution for developing multiple access WPT is having different robots take turns while exchanging power, which is also known as time division multiple access (TDMA) WPT [28], [29]. Each robot pair will have a different time slot for energy exchange, thus requiring a centralized controller for time slot assignment and synchronization.

The power transfer rate for each interaction is a direct function of the hardware ratings. As the swarm size increases, the number of time slots will also increase. Thus, for the same hardware rating, the energy transfer rate will decrease as the number of robots in the swarm increases. For instance, recharging of two robots each using a different time slot will take twice as long as a single robot recharging alone.

The number of time slots can be kept small if time slots are reused for robots operating in different areas of influence (Fig. 1). However, reusing time slots adds constraints to the movement of robots. Also, a centralized controller is now needed across neighborhoods of influence to assign new time slots.

Another alternative for multiple access WPT is frequency division multiple access (FDMA) [28], [30]. FDMA enables multiple robots to operate simultaneously by choosing different frequencies of operation. Efficient WPT requires different hardware for each frequency [31]. Thus, maintaining flexibility while increasing swarm size will proportionally increase the amount of hardware for each additional robot.

Code division multiple access (CDMA) WPT is a promising solution for developing MAET in heterogeneous swarms. The energy flow is governed by the digital codes that are used by each robot. For transmitting energy from Robot A to Robot B, A will use a transmitter code and B will use the corresponding receiver code; the other robots in the swarm will use codes that are orthogonal to both A and B. Because CDMA-WPT takes advantage of orthogonality in code space, the modulation is compact in both the time and frequency domains and thus can easily be scaled to large swarms [17]. By using appropriate shift-invariant codes, CDMA-WPT can easily be implemented without centralized control. CDMA does not constrain the movement of the robots and can enable power transfer while the robots perform their tasks. It is also easier to encrypt energy transfer, for example, by dynamically varying the codes used by each actor. The implementation of CDMA-WPT presented in this work uses efficient quasi-resonant rf circuits to create a ternary code. Although other variants of CDMA-WPT are possible, we use ternary encoding for added robustness and better hardware implementation.

III. CODE DIVISION MULTIPLE ACCESS FOR WIRELESS POWER TRANSFER

In this section, we discuss an encoding scheme, the optimization problem to obtain orthogonal codes, a simple code construction algorithm for scaling the WPT network, and the implementation details for applying CDMA-WPT to heterogeneous swarms.

Every robot in the swarm can act as both a transmitter or a receiver using the same hardware, providing energy to other robots or absorbing energy transmitted by other robots. In general, the robots can switch roles in the energy exchange by using an appropriate ternary code, and thus, can be modeled as transceivers. The behavior of CDMA-WPT is different from CDMA employed in communications. In communications, the receivers are only passive listeners and do

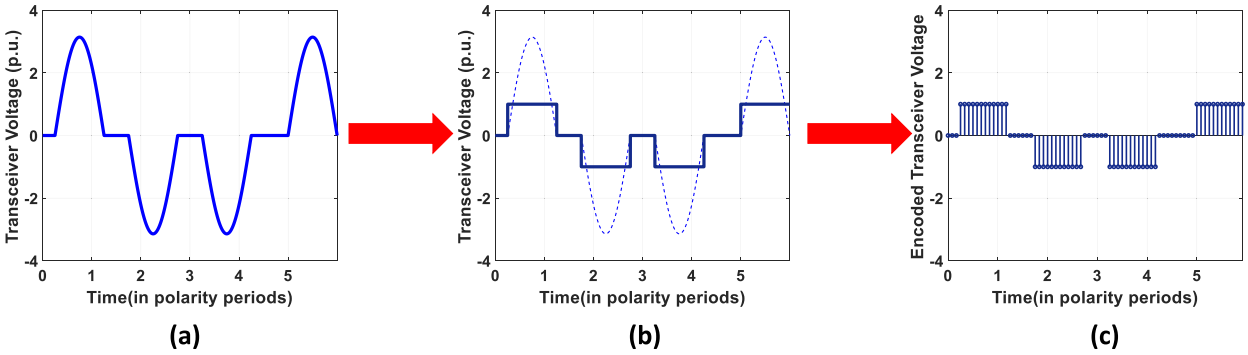

FIGURE 2. C^D transformation to obtain ternary codes corresponding to a quasi-resonant voltage. (a) The continuous-time quasi-resonant voltage output of the rf transceiver. (b) The encoded square wave pulses corresponding to the quasi-resonant voltage. (c) The ternary code from the discretization of the square pulses.

not interact with each other, and the transmitters can only send information and do not receive information from other transmitters. Thus for communications, the transmitters and receivers are unidirectional. However for WPT, transmitters and receivers are reciprocal systems, hence are bidirectional.

A. ENCODING POWER

The variant of CDMA-WPT presented here uses half sine wave pulses which are created using efficient quasi-resonant rf circuits [17], [19]. The output voltage of these circuits is a combination of positive and negative half sine wave pulses separated by zero durations Z_d. These half sine wave pulses with Z_d are encoded as a ternary code vector composed of $\{-1, 0, +1\}$ elements using the method described in this section. This encoding process preserves the orthogonality between two different output voltage waveforms, simplifies the computations involved in obtaining the orthogonal codes, and allows us to devise code construction algorithms for obtaining orthogonal codes. This process of mapping a quasi-resonant voltage to a ternary code is called C^D transformation.

Half sine wave voltage outputs from the quasi-resonant converters are used because they help eliminate the switching losses in the rf transceivers by enforcing zero voltage switching (ZVS) [32]. Using ZVS for transceivers makes them more efficient and hence improves the end-to-end energy transfer efficiency. Using quasi-resonant converters and half sine wave pulses encoded as ternary codes thus offers more efficient hardware performance and adds robustness for the implementation of CDMA-WPT. Under the following assumptions, these half sine wave voltage pulses will be encoded as ternary codes:

- All half sine wave pulses are of the same magnitude.
- The half sine wave pulses have the same duration. This duration is determined by the passive components of the transceiver and will be the same for all half sine waves of a ternary code.
- The half sine wave pulses have appropriate zero durations Z_d between them. As will be discussed later in this section, a particular choice of Z_d can make it easier to obtain receiver codes for a set of orthogonal transmitter codes.

These half sine wave pulses will be referred to as **ideal pulses**.

When operating in the steady state, the rf circuits are switched so as to produce a specific pattern of positive and negative half sine wave pulses with zero-durations between them; this pattern repeats itself after a fixed period T.

The first step to C^D transformation is to encode this pattern of half sine wave pulses into square pulses of unit magnitude

$$V_\mathrm{sq}(t) = \mathrm{sgn}(v(t)), \tag{1}$$

where $\mathrm{sgn}(\cdot)$ is the signum function, $v(t)$ is the output voltage composed of half sine wave pulses, and $V_\mathrm{sq}(t)$ are the square voltage pulses, as shown in Fig. 2(b). The second step is to discretize these square pulses to obtain a discrete time voltage vector in Fig. 2(c), which we will use as the ternary code.

A ternary code is a voltage vector that has positive half sine waves encoded as N_p $\{+1\}$ samples, the negative half sine waves encoded as N_p $\{-1\}$ samples, and zero voltages in-between encoded by an appropriate number of $\{0\}$ samples as illustrated in Fig. 2. An example ternary code for the waveform shown in Fig. 2 can be represented by the vector

$$V_1 = [\ \underbrace{0}_{Z_{\mathrm{d}1}}\ \underbrace{1111}_{+1}\ \underbrace{00}_{Z_{\mathrm{d}2}}\ \underbrace{\overline{1111}}_{-1}\ \underbrace{000}_{Z_{\mathrm{d}3}}\ \underbrace{\overline{1111}}_{-1}\ \underbrace{00}_{Z_{\mathrm{d}4}}\ \underbrace{1111}_{+1}\ ]^T,$$

where the number of samples used to represent a half sine wave is $N_\mathrm{p} = 4$. The ternary codes are periodic and the pattern repeats after the *code period* T; the time period of any polarity bit (half sine wave period) is referred to as the *polarity period*. The fraction of the total polarity period to the code period is the *duty-cycle* D of the ternary code. The total number of samples for a ternary code vector will therefore be

$$n = \frac{N \cdot N_\mathrm{p}}{D}. \tag{2}$$

For V to be a **valid code**, it must satisfy certain properties:

1) It should not have a dc component

$$\sum_{1=1}^{l} V[i] = 0, \tag{3}$$

where l is the number of samples in the ternary code.

2) It is *ternary* and can only have as its elements

$$V[i] \in \{-1,\ 0,\ 1\}. \tag{4}$$

3) It can represent intact square pulses or zero durations; in other words, N_p consecutive samples of $\{+1\}$, intact square pulses with N_p consecutive samples of $\{-1\}$, or a sequence of zeros. A ternary code not having intact square pulses, hence N_p consecutive $\{+1\}$ or $\{-1\}$ is invalid, for example for ternary codes with $N_p = 2$,

$$U = [0\ +1\ \ 0\ +1\ \ -1\ \ 0\ \ -1]^T \tag{5}$$

is **not** a valid code; however,

$$W = [0\ \underbrace{+1\ \ +1}_{+1}\ \underbrace{-1\ \ -1}_{-1}\ \ 0]^T \tag{6}$$

is a valid code.

The set of valid ternary codes is called the **valid code set** and is denoted as $\mathbb{V}$. For convenience, in the remainder of this paper, all codes will be considered valid codes.

1) POWER FLOW MODEL

The well-known voltage source model for WPT in Fig. 3 articulates the direction, magnitude, and phase of the power flow between the voltage sources v_1 and v_2 as it is applied across two interacting antennae. We extend this model through the C^D transformation to articulate the direction and magnitude of the power flow of codes. It is worth noting that this model extension to codes in the range of the C^D transformation preserves direction and orthogonality characterized by zero power flow, but not necessarily power magnitude, for a class of time domain voltage waveforms of which ideal half sine wave pulses are a member.

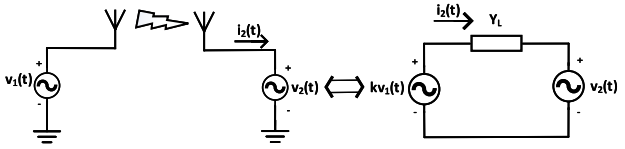

FIGURE 3. Voltage source model for understanding power flow in a general WPT system. The two transceivers are abstracted as voltage sources driving the interacting antennae. To derive a power flow model, the Thevenin equivalent circuit at either terminal can be used. The voltage source, kv_1 represents the scaled Transceiver 1 voltage when observed from the opposing terminal; Y_L represents the link admittance operator that corresponds to the link and antennae properties.

The wireless power transfer link in Fig. 3 is modeled as two Thevenin equivalent voltage sources $kv_1(t)$ and $v_2(t)$ for Transceivers 1 and 2 respectively, with an intervening lossless admittance Y_L. The current in Transceiver 2 is given by

$$\begin{aligned} i_2 &= Y_\mathrm{L}(kv_1 - v_2) \\ &= i_{21} + i_{22}, \end{aligned} \tag{7}$$

where k is the factor by which the voltage of Transceiver 1 scales as it traverses the WPT link; $Y_\mathrm{L}(\cdot)$ is the link admittance operator that acts on the voltages. Thus, i_{21} is the current contribution due to the voltage of Transceiver 1 and i_{22} is the current contribution due to the voltage of Transceiver 2. For an inductive link having a voltage $v(t)$ applied across the link, the link admittance operator acts on the voltage difference as

$$Y_\mathrm{L}\, v(t) = \frac{1}{L_{\mathrm{Y1}}} \int_0^t v(\tau)\, d\tau, \tag{8}$$

where L_{Y1} is the link inductance. Using (8), the current at the Transceiver 2 terminal is given by

$$i_2(t) = \int_0^t \frac{kv_1(\tau) - v_2(\tau)}{L_{\mathrm{Y1}}}\, d\tau. \tag{9}$$

The power transferred from Robot 1 to Robot 2 is

$$p_{12} = \frac{1}{T} \int_0^T kv_1(t)\, i_2(t)\, dt, \tag{10}$$

where T is the code period of the two transceivers. The power transferred can also recognized as the projection of the current I_2 onto the voltage V_1. Only the current components that are aligned with the voltage transfer real power; whereas, the current components that are orthogonal to the voltage only contribute reactive power (oscillating) power between the two transceivers. Thus, the power transferred can be expressed as an inner product of the voltage with the current

$$\begin{aligned} p_{12} &= \langle kv_1(t),\ i_2(t) \rangle \\ &= \langle kv_1(t),\ i_{22}(t) \rangle, \end{aligned} \tag{11}$$

where $\langle \cdot\,, \cdot \rangle$ is the inner product [33]. Because the admittance is assumed to be lossless, the current component i_{21} will be orthogonal to the voltage v_1.

In the C^D domain, the voltages from Transceivers 1 and 2 are denoted V_1 and V_2 and the currents I_1 and I_2, respectively. It is worth noting that V_1 and V_2 are ternary code vectors. The current due to the voltage of Transceiver 2 is given by

$$I_{22}[n] = I_{22}[n-1] + \frac{1}{L_{\mathrm{Y1}}} \sum_{i=1}^{n} (-V_2[i])\,. \tag{12}$$

The ternary codes, V_1 and V_2 have no dc component (zero average value), hence the dc component of the current I_2 will not alter the power flow analysis; therefore, $I_{22}[0] = 0$. Using (12), the current vector corresponding to the voltage ternary code can be expressed as

$$\begin{aligned} I_{22} &= -\frac{1}{L_{\mathrm{Y1}}} \begin{bmatrix} 1 & 0 & \cdots & \cdots & 0 \\ 1 & 1 & 0 & \cdots & 0 \\ 1 & 1 & 1 & \cdots & 0 \\ \vdots & & & & \\ 1 & 1 & 1 & \cdots & 1 \end{bmatrix} V_2 \\ &= AV_2, \end{aligned} \tag{13}$$

where the matrix A is the admittance operator in the C^D domain and is analogous to the linear integral operator used in (9). The matrix A maps a valid ternary code vector $V \in \mathbb{V}$ of length n to a real current vector $I \in \mathbb{R}^n$

$$A\colon\ \mathbb{V} \mapsto \mathbb{R}^n.$$

When representing the voltage and current signal in the C^D domain, the power transferred can be obtained as

$$\begin{aligned} P_{12} &= \frac{1}{N}\langle kV_1, I_2\rangle \\ &= \frac{1}{N}\langle kV_1, AV_2\rangle. \end{aligned} \tag{14}$$

2) ORTHOGONAL CODES

Two ternary codes, V_1 and V_2 are orthogonal to each other if they do not exchange power between them, i.e. $P_{12} = 0$. For a given ternary code $V_1 \in \mathbb{V}$, the orthogonal ternary code V_2 that neither receives nor transmits power can be obtained by

$$\begin{aligned} &\underset{V_2}{\text{minimize}} |P_{12}| = |[\,|\rangle\langle V_1, AV_2\rangle \\ &\text{subject to } V_2 \in \mathbb{V}, \\ &\qquad \|V_2\|_1 = \|V_1\|_1 , \end{aligned}$$

where $\|\cdot\|_1$ is the 1-norm and $\mathbb{V}$ represents the set of valid ternary codes. The first constraint in the optimization ensures that V_2 is a valid ternary code; the second constraint ensures that the number of pulses in V_1 and V_2 are equal. This optimization problem has a convex objective function, but the first constraint of ensuring that V_2 is a valid code is a mixed integer, non-convex constraint, which in general is hard to solve and often requires resorting to global optimizers like genetic algorithms (GA). In order to create an energy network, a large number of orthogonal codes may be needed. Although, it is possible to obtain multiple codes using a GA, the method is not as straightforward to scale. The simple code construction algorithm in the next section is easily scalable [20].

3) CODE CONSTRUCTION ALGORITHM FOR OBTAINING ORTHOGONAL TERNARY CODES

The code construction algorithm (CCA) assumes that two orthogonal codes are already known and then provides a simple method of finding more orthogonal codes. The initial orthogonal codes can be obtained by starting with a ternary code and then solving the optimization problem described above. To apply CCA, we first need to define an element-wise concatenation operation between two sets, $S_a = \{A_1, A_2, \ldots, A_N\}$ and $S_b = \{B_1, B_2, \ldots, B_N\}$ having an equal number of valid codes N. The length of codes for set S_a is n_a and the length of codes for the set S_b is n_b, respectively.

Definition 1 (Orthogonal Set): A code set $S = \{V_1, V_2, \ldots, V_N\}$ is an orthogonal set if

$$\langle V_i, A\, V_j\rangle = 0, \quad \forall i \neq j. \tag{15}$$

Definition 2 (Concatenation Operation): The concatenation operation is defined as

$$S_c = S_a \sqcup S_b = \{A_1B_1, A_2B_2, A_3B_3, \ldots, A_NB_N\}. \tag{16}$$

Remark: Since A_i and B_i are both valid codes $\forall i$, $C_i = A_iB_i$ is also a valid code.

Remark: The length of the codes of set S_c will be $n_c = n_a + n_b$, where n_a and n_b are lengths of the codes of set S_a and S_b.

Definition 3: Code Negation: The negation of a code V is defined as

$$\overline{V} = -V. \tag{17}$$

As an illustration, consider a ternary code

$$W = [0 \;\; +1 \;\; +1 \;\; -1 \;\; -1 \;\; 0]^T; \tag{18}$$

the negation of code W is

$$\overline{W} = [0 \;\; -1 \;\; -1 \;\; +1 \;\; +1 \;\; 0]^T. \tag{19}$$

Definition 4: Negation of a Set: The negation of a code set $S = \{V_1, V_2, \ldots, V_N\}$ is defined as

$$\overline{S} = \left\{\overline{V_1}, \overline{V_2}, \ldots, \overline{V_N}\right\}. \tag{20}$$

Theorem 5: For an orthogonal set $S_1 = \{V_1, V_2, \ldots, V_N\}$ with N codes, the set S_2 created from the self-concatenation of S_1

$$S_2 = \left\{S_1 \sqcup S_1, S_1 \sqcup \overline{S_1}\right\} \tag{21}$$

will be an **orthogonal set** with $2N$ elements.
The elements of the set S_2 will be

$$S_2 = \left\{V_1V_1, V_2V_2, \ldots, V_nV_n, V_1\overline{V_1}, V_2\overline{V_2}, \ldots, V_N\overline{V_N}\right\}. \tag{22}$$

Thus, two orthogonal codes V_i and V_j will generate four orthogonal codes: $[V_i\ V_i]$, $[V_i\ \overline{V_i}]$, $[V_j\ V_j]$, and $[V_j\ \overline{V_j}]$. The proof follows from the following Lemmas.

Lemma 6: The codes $[V_i\ V_i]$ and $[V_j\ V_j]$, both created by the concatenation of two orthogonal codes V_i and V_j are orthogonal.

Proof: The two codes V_i and V_j are orthogonal to each other, hence

$$\langle V_i, A_k V_j\rangle = 0, \tag{23}$$

where A_k is the admittance operator in the C^D domain corresponding to the codes V_i and V_j. As the codes are concatenated, the matrix A_{k+1} will become

$$A_{k+1} = \begin{bmatrix} A_k & 0 \\ \mathbb{1} & A_k \end{bmatrix}, \tag{24}$$

where 0 is a zeros matrix of the appropriate size and $\mathbb{1}$ is a ones matrix of the appropriate size. So the power flow between the codes $[V_i\ V_i]$ and $[V_j\ V_j]$ will be

$$\begin{aligned} P_{ij} &= \langle [V_i\ V_i],\ A_{k+1}[V_j\ V_j]\rangle \\ &= V_i^T A_k V_j \ + \ V_i^T \mathbb{1} V_j \ + \ V_i^T A_k V_j \\ &= 0. \end{aligned}$$

The term $V_i^T \mathbb{1} V_j = 0$ because V_j is a valid ternary code and $V_i^T A_k V_j = 0$ because V_i and V_j are orthogonal to each other. Hence, the two codes $[V_i\ V_i]$ and $[V_j\ V_j]$ are orthogonal. □

Lemma 7: The codes $[V_i\ V_i]$ and $[V_j\ \overline{V_j}]$ are orthogonal.

Proof: The power flow between the codes $[V_i\ V_i]$ and $[V_j\ \overline{V_j}]$ will be

$$\begin{aligned} P_{i\bar{j}} &= \langle [V_i\ V_i],\ A_{k+1}[V_j\ \overline{V_j}] \rangle \\ &= V_i^T A_k V_j\ +\ V_i^T \mathbb{1} V_j\ -\ V_i^T A_k V_j \\ &= 0. \end{aligned}$$

So, the two codes $[V_i\ V_i]$ and $[V_j\ \overline{V_j}]$ are orthogonal. □

Lemma 8: The codes $[V_i\ \overline{V_i}]$ and $[V_j\ \overline{V_j}]$ are orthogonal.

Proof: The power flow between the codes $[V_i\ \overline{V_i}]$ and $[V_j\ \overline{V_j}]$ will be

$$\begin{aligned} P_{\bar{i}\bar{j}} &= \langle [V_i\ \overline{V_i}],\ A_{k+1}[V_j\ \overline{V_j}] \rangle \\ &= V_i^T A_k V_j\ -\ V_i^T \mathbb{1} V_j\ +\ V_i^T A_k V_j \\ &= 0. \end{aligned}$$

The term $V_i^T A_k V_j = 0$ because the two codes V_i and V_j are orthogonal. □

Lemma 9: The codes $[V_i\ \overline{V_i}]$ and $[V_j\ V_j]$ are orthogonal.

Proof: The power flow between the codes $[V_i\ \overline{V_i}]$ and $[V_j\ V_j]$ will be

$$\begin{aligned} P_{\bar{i}j} &= \langle [V_i\ \overline{V_i}],\ A_{k+1}[V_j\ V_j] \rangle \\ &= V_i^T A_k V_j\ -\ V_i^T \mathbb{1} V_j\ -\ V_i^T A_k V_j \\ &= 0. \end{aligned}$$

The term $V_i^T A_k V_j = 0$ because the two codes V_i and V_j are orthogonal. So, the two codes $[V_i\ \overline{V_i}]$ and $[V_j\ V_j]$ are orthogonal. □

Lemma 10: The codes $[V_i\ V_i]$ and $[V_i\ \overline{V_i}]$ are orthogonal.

Proof: The power flow between the codes $[V_i\ V_i]$ and $[V_i\ \overline{V_i}]$ will be

$$\begin{aligned} P_{i\bar{i}} &= \langle [V_i\ V_i],\ A_{k+1}[V_i\ \overline{V_i}] \rangle \\ &= V_i^T A_k V_i\ +\ V_i^T \mathbb{1} V_i\ -\ V_i^T A_k V_i \\ &= 0. \end{aligned}$$

The term $V_i^T \mathbb{1} V_i = 0$ because V_i is a valid ternary code. Hence, the two codes $[V_i\ V_i]$ and $[V_i\ \overline{V_i}]$ are orthogonal. □

Hence, the two codes V_i and V_j lead to four orthogonal codes of twice the length using the concatenation operation. Now, starting with an orthogonal set, $S_1 = \{C_1,\ C_2\}$, use Algorithm 1 to obtain a set of N orthogonal codes. It is worth noting that the algorithmic complexity grows as $\mathcal{O}(\log n)$, and thus is easily scalable.

Algorithm 1 Code Construction Algorithm for Scaling CDMA-WPT to Include N Transceivers

Result: N orthogonal ternary codes
Start with a set of 2 orthogonal codes, $S_1 = \{C_1,\ C_2\}$ of length 2^k; $i = 1$;
while $i \leq \log_2 N - 1$ **do**
  Construct codes of length 2^{k+1} by concatenating set S_i with itself and S_i with $-S_i$;
  $S_{i+1} = \{S_i \sqcup S_i,\ S_i \sqcup -S_i\}$;
  $i = i + 1$;
end

4) RECEIVER CODES

The output of CCA will be an orthogonal code set S_m with $m \geq N$ orthogonal codes. To enable power transfer from these ternary codes, receiver codes are required to receive power from the transmitter. The receiver codes corresponding to a set of orthogonal transmitter codes must have the following properties:

1) All the codes should be valid.
2) Every receiver code should be orthogonal to the other receiver codes.
3) Every receiver code should be orthogonal to the other transmitter codes.
4) Every receiver code should maximize the power transferred from its corresponding transmitter.

a: ORTHOGONALITY OF RECEIVERS

The receiver codes that maintain orthogonality of the corresponding transmitter codes and satisfy the properties of a valid code are called **valid receiver codes**. A straightforward choice for a valid receiver code is to have all receiver codes bearing a linear relationship with their corresponding transmitter codes

$$V_{\mathrm{R}i} = SV_i, \tag{25}$$

where $V_{\mathrm{R}i}$ is the receiver code corresponding to transmitter code V_i and S is a matrix. In general, it is hard to find receiver codes that maintain orthogonality among themselves and also to the other transmitters. However, for the special case where $Z_{\mathrm{d}i} \geq \frac{N_{\mathrm{p}}}{2}$ for every ternary code and the receiver codes are shifted versions of the corresponding transmitter codes, where shift $s \leq \frac{N_{\mathrm{p}}}{2}$ samples, the receiver codes will be orthogonal to the other transmitter codes. In this case, the matrix S corresponds to a rotation and these special codes comprise the set $\mathbf{C_2}$.

b: RECEIVING POWER

In general, the inner product is not necessarily preserved under the C^D transformation. So, the analysis for power received is performed in the continuous time domain with underlying ideal half sine waves pulses. A perfect receiver produces a current that is congruent to the transmitter voltage so that

$$i_2 = Y_{\mathrm{L}} v_2 = i_{\mathrm{M}} \frac{v_1}{\|v_1\|_2}, \tag{26}$$

where i_{M} represents the maximum magnitude of current that the transceiver hardware can produce as shown in Fig. 4. However, hardware constraints that enforce ZVS do not allow the transceiver to produce this current. At higher frequencies (≥ 1 MHz), it is necessary to enforce ZVS to ensure that the switching losses are not overwhelming. So, the actual receiver codes must satisfy the constraints imposed by ZVS.

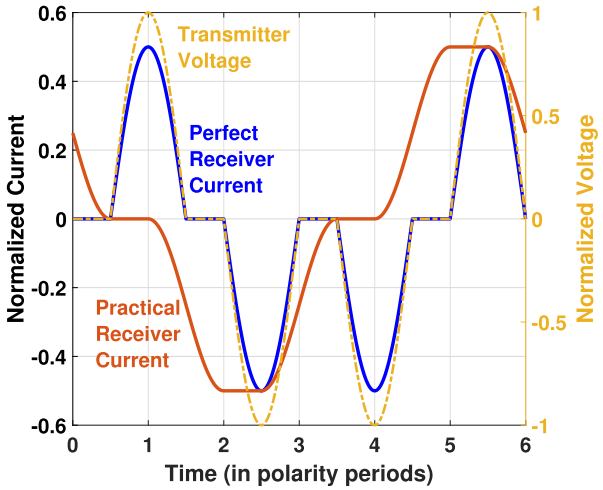

FIGURE 4. Comparison of perfect (unconstrained) current and the practical (actual) receiver current. Perfect current for WPT lines up perfectly with the transmitter voltage, thus maximizing power transfer; this is not possible with hardware ZVS constraints. The optimal practical current maximizes the power transfer while satisfying ZVS constraints.

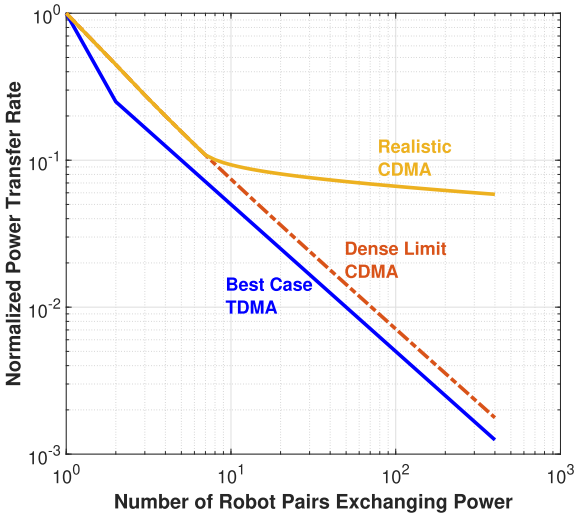

FIGURE 5. Charging rate comparison for TDMA and CDMA as the number of robot pairs increases. Dense CDMA assumes strong WPT connectivity between every robot, whereas realistic CDMA assumes a decreasing connectivity among the robots as the swarm size increases. Even for the best case TDMA, the charging rate decreases as $\frac{1}{2N}$, whereas for dense limit CDMA, the rate of decrease is $\frac{1}{\sqrt{2N}}$.

Additionally, if the receiver codes belong to $\mathbf{C_2}$, the needed orthogonality conditions are satisfied. It is a well-known fact that for two single frequency voltage sources connected by a purely reactive impedance, the maximum power transfer occurs when the two sources have a phase difference of 90 degrees [34]. Hence, if the transmitter ternary codes are $\mathbf{C_2}$, in other words restricted to $Z_{di} \geq \frac{N_p}{2}\ \forall\, i$, then through ac circuit analysis, the optimal receiver code is also

$$V_2 = SV_1, \tag{27}$$

where S is the same matrix that corresponds to a rotation of $\frac{N_p}{2}$ samples.

Using (27), the valid receivers corresponding to the transmitters of orthogonal code set S_N created by CCA can be obtained. These N receivers can only be powered by their corresponding transmitters and will not exchange power with other transmitters or receivers. Thus, when used in a large heterogeneous swarm, N robots with $\mathbf{C_2}$ transmitter codes can power N robots with $\mathbf{C_2}$ receiver codes at the same time regardless of their relative physical positions among other transceivers.

5) CODE CONSTRUCTION ALGORITHM PERFORMANCE

The CCA exploits the orthogonality in code space to create a large set of orthogonal ternary codes. Having obtained the transmitter and receiver codes for an orthogonal network, we can now analyze the charging rates for different robots in heterogeneous swarms exchanging energy using CDMA-WPT as the swarm size increases. For a comparison, the charging rates of the TDMA approach employing P2P power transfer are also analyzed. Figure 5 compares the theoretical results for CDMA-WPT and TDMA-WPT. It is assumed that all transceivers used in the power exchange have the same power rating. In the best case scenario with no added hardware constraints, the charging rate for TDMA decreases at the rate of $\frac{1}{2N}$, with N being the number of robots pairs exchanging power; whereas, the charging rate for a dense CDMA-WPT goes down at the rate of $\frac{1}{\sqrt{2N}}$. A dense CDMA assumes that all the robots in the swarm have strong WPT connectivity to each other. However, in reality there is a limit to the number of robots that can fit within a physical volume and the wireless connectivity of the robots falls of with the distance as had been illustrated in Fig. 1. Thus taking into account these realistic considerations, the charging rate for a realistic CDMA-WPT saturates to an almost constant value as the number of robots increases.

B. HARDWARE DESCRIPTION

The basic hardware building blocks for implementing CDMA-WPT include: (1) a switching rf power amplifier; (2) a switching controller with a library of codes for an orthogonal network; and (3) an appropriate antenna based on the chosen switching frequency of operation and the spectrum of the ternary codes [35].

The methods described in this paper are applicable to both near-field and far-field WPT; however, we present a near-field implementation of the concept using coupled inductors at a switching frequency of 100 MHz or lower. Fig. 6 shows a basic block diagram for enabling energy transfer between two robots. The switching controller creates the switching pattern in the rf power amplifier for the pertinent ternary code. This switching sequence can either be stored in the controller as a library of transmitter and receiver codes or created on the fly. However, creating codes on the fly requires both time and energy, hence it often preferable to use data storage within each controller to maintain a library of the ternary codes.

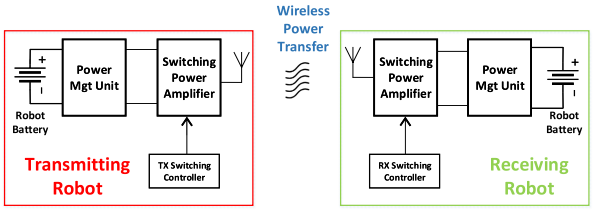

FIGURE 6. Block diagram showing the important components needed for enabling two robots to exchange power through CDMA-WPT. Each robot is equipped with an appropriate antenna, a switching amplifier capable of converting dc to rf and vice versa, and a controller capable of switching the amplifier to create the desired ternary codes.

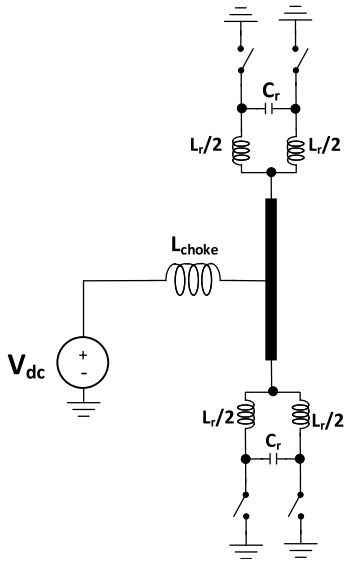

FIGURE 7. X-CMCD switching power amplifier for realizing ternary codes. The amplifier is capable of converting dc power from the battery to rf power that is used to drive the antenna and vice versa.

Each robot in CDMA-WPT is capable of sending and receiving power, thus acting as a transceiver. Thus, the rf amplifier used for WPT must be capable of converting dc power to rf and vice-versa. The amplifier must also be capable of realizing the ternary codes obtained using the code construction algorithm. Figure 7 shows the X-CMCD power amplifier that can be used in the transceiver for implementing CDMA-WPT [17]. The X-CMCD amplifier is derived from the well-known current-mode class-D (CMCD) power amplifier [36]; it consist of two CMCDs connected in a push-pull manner to create positive and negative half sine waves.

IV. DESIGN EXAMPLES WITH CDMA-WPT

In this section, we present the application of CDMA-WPT to heterogeneous swarms with 4 robots in hardware and 30 robots in simulation.

A. HARDWARE DEMONSTRATION OF MULTIPLE ACCESS ENERGY TRANSFER IN FOUR ROBOTS

First consider the case of a heterogeneous swarm with four robots. An example could be the swarmanoid in [2] with two footbots and two handbots or the convoy in [37] with two supply units and two defender units. We need these robots to

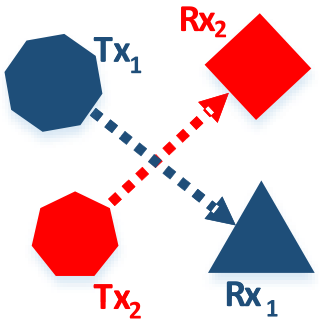

FIGURE 8. Heterogeneous robot swarm with four robots. The robots RX_1 and RX_2 are running low on battery and hence need to receive energy from TX_1 and TX_2, respectively. The energy transfer should not be affected by the proximity of the other robots in the space, i.e. TX_1 should only transmit power to RX_1 and TX_2 should only transmit power to RX_2.

be able to exchange energy among each other as and when needed. Because there are four robots, we need two sets of orthogonal codes because at most, we can have a scenario where all four robots are in close proximity and needing to exchange energy as illustrated in Fig. 8. For the proof of concept, we selected the code vectors

$$C_1 = [0\ +1\ +1\ 0\ -1\ -1\ 0\ +1\ +1\ 0\ -1\ -1]^T$$
$$C_2 = [0\ +1\ +1\ 0\ +1\ +1\ 0\ -1\ -1\ 0\ -1\ -1]^T$$

and a constant zero-duration equal to half the polarity period. The receiver codes for these transmitters will be shifted versions of the transmitter codes. Each robot will have all four transmitter and receiver codes; depending on the energy exchange desired by each robot's controller, the appropriate ternary code will be used. The X-CMCD transceiver described in section III-B was used for driving the antennae for the four robots. For an implementation in the actual robots, each robot will have an X-CMCD transceiver and an antenna.

Figure 9 shows how the codes are realized by the transceiver hardware. To verify the power-flow selectivity, the dedicated transmitter receiver pairs are kept at a distance of 1.5 cm from each other and the distance between the two pairs exchanging energy is varied. The distance between TX_1 and RX_1, and between TX_2 and RX_2 is maintained constant at 1.5 cm. This mimics the scenario where the two robots exchanging energy remain close to each other while the other robots in the environment could still be moving. Table 1 shows the relatively constant dc-dc power transfer from TX_1 to RX_1 and from TX_2 to RX_2. The dc power levels shown in Table 1 correspond to battery charging and discharging rates. The maximum variation in the power level is only 10 % even when the two WPT networks are very close to each other. The small variation in the power level occurs because of some distortion in the transceiver waveforms. It is worth noting that this can be considered a general scenario for WPT: the cases where one robot has to receive energy from two other robots or one robot has to power two other robots can be performed by using a transmitter code for the transmitting robots and the corresponding receiver codes for the receiving robots.

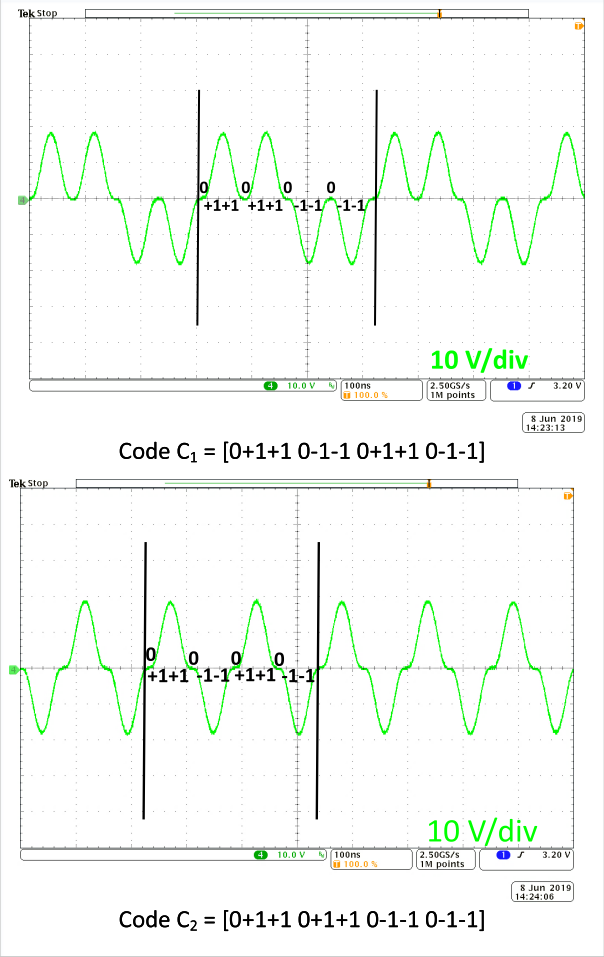

FIGURE 9. Realization of ternary codes in hardware. Notice that the oscilloscope waveforms are high-power signals with a magnitude of ∼20 V.

TABLE 1. Hardware results for power variation for all transceivers as the distance between the networks TX_1RX_1 and TX_2RX_2 is varied.

Distance (cm)	Tx1 (W)	Rx1 (W)	Tx2 (W)	Rx2 (W)
6.2	7.43	5.62	7.71	5.35
4.8	7.42	5.57	7.72	5.33
3.8	7.50	5.60	7.82	5.36
2.3	7.28	5.41	7.43	5.19
1.3	7.17	5.28	7.57	5.05
0.9	7.03	5.13	7.52	4.92
0.6	6.96	5.05	7.51	4.86

B. HETEROGENEOUS SWARMS WITH 30 ROBOTS

One of the advantages of CDMA-WPT for heterogeneous swarms is the ease of scalability towards hundreds and possibly thousands of devices. To illustrate a simple example of a real world implementation, a heterogeneous swarm with 30 robots is considered. The exact structure of the ad-hoc energy network will depend on the size and capabilities of the robotic swarm. Accounting for these energy networks during the planning process, in the control algorithms [38], and in resource allocation is an area of promising future research. Depending on the resources available to the robots in the swarm, it may be desirable to form one kind of network over the other. We present two different energy networks as examples of enabling energy exchange in robotic swarms with 30 robots.

1) SWARMS WITH PEER-TO-PEER CHARGING

First consider the case of a robotic swarm with identical energy storage and identical transceivers so that a robot is only able to power one other robot at any given time as shown in Fig. 10. At any given time during the particular mission, there can be at most 15 robots transferring energy to the remaining 15 robots.

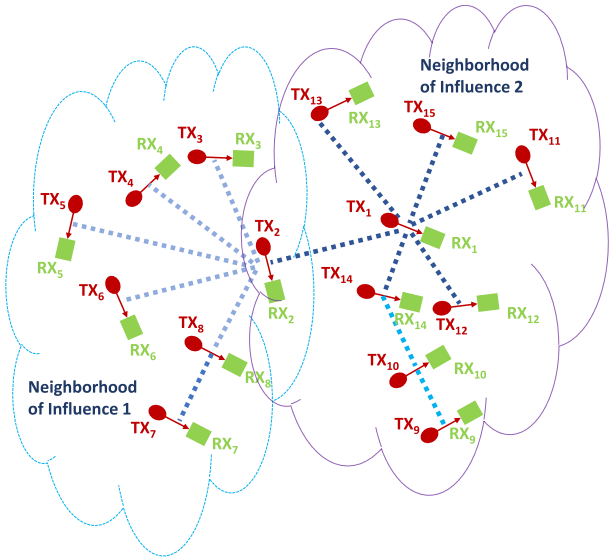

FIGURE 10. Robot swarm with 30 robots with 15 transmitter-receiver pairs exchanging energy. The interference in the energy exchange is caused by the other transmitter-receiver (TRX) pairs near the intended TRX pair exchanging power. The maximum interference that a particular TRX experiences is bounded by modeling two neighborhoods of influence. By using appropriate orthogonal codes, the effects of interference between the TRX pairs are minimized.

This swarm requires a code set of at least 15 orthogonal codes. These codes are created apriori using Algorithm 1 and stored in memory within each robot. Now based on the energy needs of a particular robot and the neighborhood robots, a robot can realize a transmitter or receiver code to enable exchange energy with its neighbors. For a successful energy transfer, a robot only has to synchronize with its dedicated transmitter or receiver, thus needing access to local information only. The other robots in the neighborhood only add interference, which is avoided by using different codes for each power exchange link. Figure 10 shows the 30 robots at a given instance with the neighboring transmitter-receiver pair exchanging energy.

Two neighborhoods of influence are illustrated in Fig. 1. Transmitter-receiver (TRX) pairs within the same neighborhood act as sources of interference. It is important to point out that the neighborhoods of influence merely represent an upper bound on the interference that a particular TRX pair can have during power exchange; the TRX robot pairs can move from one neighborhood of influence to another. Thus, the neighborhoods of influence do not constrain the

movement or location of the robots by any means. Rather, neighborhoods of influence provide a more realistic model of interference. In this example, we bounded the the maximum number of robots interfering in the energy exchange for each TRX pair.

TABLE 2. Simulation results for power variation of the transmitters shown in Fig. 10. The use of appropriate orthogonal codes keeps the power variation under 0.1 W (≤ 0.5%).

	Without Interference	With Interference
P_{TX2}	21.36 W	21.45 W
P_{TX3}	21.37 W	21.41 W
P_{TX4}	21.36 W	21.36 W
P_{TX5}	21.52 W	21.57 W
P_{TX6}	21.63 W	21.63 W
P_{TX7}	22.00 W	22.00 W
P_{TX8}	21.40 W	21.40 W
P_{TX9}	21.49 W	21.49 W
P_{TX10}	21.41 W	21.41 W
P_{TX11}	21.41 W	21.41 W
P_{TX12}	21.40 W	21.40 W
P_{TX13}	21.60 W	21.60 W
P_{TX14}	21.57 W	21.57 W
P_{TX15}	21.54 W	21.54 W

Each transmitter is assigned a different orthogonal code with the corresponding receiver assigned a receiver code as defined using (27). Table 2 shows a comparison of the transmitter input powers with and without interference. The maximum variation of power transfer from a transmitter to its receiver is less than 0.5%. Hence, using orthogonal codes for each TRX pair, the interference between different pairs is avoided and power transfer occurs in a similar way to the transmitter-receiver pair exchanging power in isolation, demonstrating power flow selectivity. It is also worth noting that the power transfer depends solely on the strength of power signals between TRX pairs and not on the other robots in the neighborhood. Therefore, the TRX pairs can move around with only an insignificant perturbation in the power transfer.

2) HETEROGENEOUS SWARM WITH HIGHER POWER TRANSFER CAPABILITIES

In the previous section, every robot in the swarm was only capable of transmitting and receiving the same the quantity of power, hence the power transmitted or received by each robot was nearly identical (≈21.5 W). However, in heterogeneous swarms, some robots in the swarm can have the capability of transmitting or receiving varying amounts of power. The power transfer capability of each robot can be included as part of the planning process and be considered as a design variable in the determination of control policy. We can take advantage of this higher power availability to enable faster charging of some robots. To demonstrate its effectiveness, we considered a heterogeneous swarm of 30 robots with some robots having a power capability with as much as seven times that of the smallest robot.

For an illustration of a particular mission at a given time, the robots form a scale-free network with 30 nodes, as shown in Fig. 11. The robots connected through a scale-free network

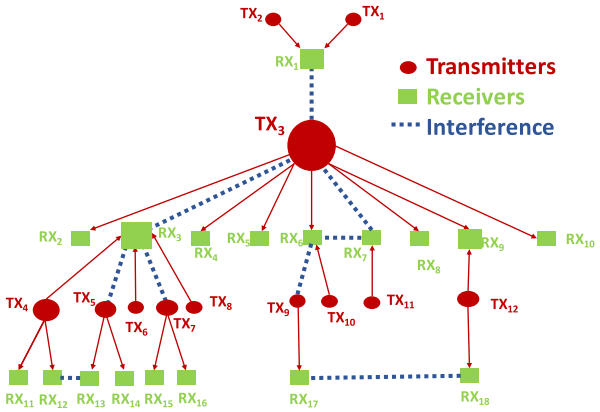

FIGURE 11. Heterogeneous robot swarm with 30 robots forming a scale-free ad-hoc energy network, generated using the BA algorithm [39]. The red nodes denote the energy rich robots transferring energy to the green nodes. The robots are assigned transmitter and receiver codes based on their neighbors. Due to the nature of the mission, there is unavoidable interference. By using appropriate orthogonal codes, the effect of interference is eliminated or minimized.

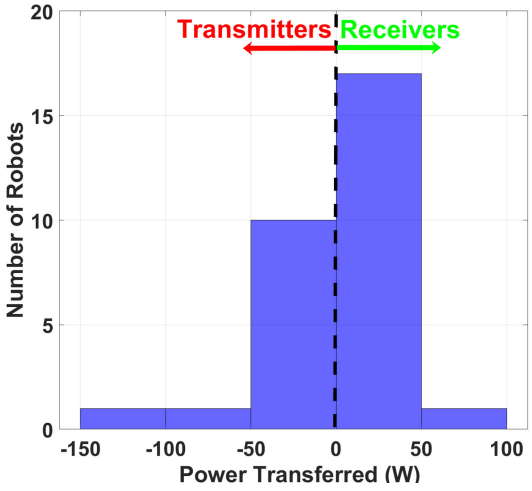

FIGURE 12. Numerical results showing power distribution among robots within the ad-hoc scale-free energy network formed by the heterogeneous swarm. The negative powers denote the power sent by a transmitter and the positive powers denote receiver powers.

are a very good example of the realistic CDMA scenario modeling the limited area of the neighborhood of influence. It is assumed that the robots are connected to their immediate neighbors and as the size of the swarm increases, the connectivity of the robots reduces in number, thus imposing limits to the number of robots interacting with each other at any given time as shown in Fig. 1.

Based on the state of charge (energy) of the batteries, the robots exchange energy. The transmitters in the network use the transmitter codes, while the receivers use the corresponding receiver codes. To minimize the effects of interference from other robots, appropriate orthogonal codes are used. For example, the transmitter codes for TX_1 and TX_3 are orthogonal which ensures that despite RX_1 being near TX_3, there is no energy exchange between the two. Figure 12 shows the histogram of the numerical results for the

TABLE 3. Simulation results for power variation of the transmitters shown in Fig. 11. The use of appropriate orthogonal codes keeps the power variation under 0.1 W. The robot TX_3 transmits seven times the power of a single transmitter.

	Without Interference	With Interference
P_{TX1}	21.33 W	21.33 W
P_{TX2}	21.33 W	21.33 W
P_{TX3}	149.52 W	149.59 W
P_{TX4}	64.11 W	64.11 W
P_{TX5}	42.72 W	42.72 W
P_{TX6}	21.37 W	21.37 W
P_{TX7}	43.04 W	42.93 W
P_{TX8}	21.37 W	21.37 W
P_{TX9}	21.63 W	21.63 W
P_{TX10}	21.36 W	21.30 W
P_{TX11}	22.00 W	22.00 W
P_{TX12}	42.72 W	42.72 W

calculated power transferred to each robot. The robot power transfer depends on the number of other robots with which it is interacting. Each interaction corresponds to approximately 21.5 W of power transferred; thus, based on the number of robots connected, different robots exchange different power.

It is worth recalling that interference has the potential to affect both transmitters and receivers. Appropriate orthogonal codes minimize the effect of interference on wireless power transfer.

For the configuration in Fig. 11, 12 robots in the swarm act as transmitters and the remainder 18 robots as receivers. Table 3 compares the transmitter power distribution in the swarm with versus without interference. One can observe that by using appropriate orthogonal codes, the effects of interference on power variation are minimized. From the table, it can also be observed that the transmitters TX_3, TX_4, TX_5, TX_7, and TX_{12} transfer power to more than one robot as their power transfer capabilities allow.

TABLE 4. Simulation results for power variation of the receivers shown in Fig. 11. The use of appropriate orthogonal codes keeps the power variation under 0.1 W.

	Without Interference	With Interference
P_{RX1}	42.65 W	42.65 W
P_{RX2}	21.36 W	21.36 W
P_{RX3}	64.11 W	64.04 W
P_{RX4}	21.36 W	21.36 W
P_{RX5}	21.36 W	21.36 W
P_{RX6}	42.72 W	42.72 W
P_{RX7}	22.00 W	22.02 W
P_{RX8}	21.36 W	21.36 W
P_{RX9}	42.72 W	42.72 W
P_{RX10}	21.37 W	21.37 W
P_{RX11}	21.36 W	21.36 W
P_{RX12}	21.37 W	21.36 W
P_{RX13}	21.36 W	21.36 W
P_{RX14}	21.36 W	21.36 W
P_{RX15}	21.52 W	21.52 W
P_{RX16}	21.52 W	21.52 W
P_{RX17}	21.36 W	21.63 W
P_{RX18}	21.36 W	21.36 W

Table 4 shows the power of different receiver robots within the swarm. It can clearly be observed that the use of orthogonal codes minimizes the effects on the power received by the different receivers. Also, based on the number of transmitter robots with which a receiver interacts, some receivers are able to receive up to three times more power than from a single transmitter alone.

V. CONCLUSION

Energy is one of the key enablers for robotic swarms. The feasibility of heterogeneous swarms to perform complex missions depends upon the energy stored in the robot batteries. Allowing multiple access energy transfer (MAET) in robot swarms provides more flexibility to deal with uncertain missions. In this paper, we presented an implementation of CDMA-WPT for enabling MAET in heterogeneous swarms. The encoding scheme, power flow model, and code construction algorithm are presented for the chosen implementation. The application of CDMA-WPT to a heterogeneous swarm with four robots was demonstrated in hardware achieving 5 W of virtually constant power transfer from transmitters to receivers regardless of the presence of neighboring interfering robots. Finally, the application of CDMA-WPT was demonstrated in simulations of a heterogeneous swarm with 30 robots connected through a scale free network achieving the desired levels of power transfer in the robots while avoiding interference from neighbors.

REFERENCES

[1] M. Brambilla, E. Ferrante, M. Birattari, and M. Dorigo, "Swarm robotics: A review from the swarm engineering perspective," *Swarm Intell.*, vol. 7, no. 1, pp. 1–41, Mar. 2013.
[2] M. Dorigo *et al.*, "Swarmanoid: A novel concept for the study of heterogeneous robotic swarms," *IEEE Robot. Autom. Mag.*, vol. 20, no. 4, pp. 60–71, Dec. 2013.
[3] A. Babić, F. Mandić, G. Vasiljević, and N. Mišković, "Autonomous docking and energy sharing between two types of robotic agents," *IFAC-PapersOnLine*, vol. 51, no. 29, pp. 406–411, 2018.
[4] M. Carrillo, I. Gallardo, J. Del Ser, E. Osaba, J. Sanchez-Cubillo, M. N. Bilbao, A. Gálvez, and A. Iglesias, "A bio-inspired approach for collaborative exploration with mobile battery recharging in swarm robotics," in *Proc. Int. Conf. Bioinspired Methods Appl.* Paris, France: Springer, 2018, pp. 75–87.
[5] S. C. Mukhopadhyay, G. S. Gupta, and B. J. Lake, "Design of a contactless battery charger for micro-robots," in *Proc. IEEE Instrum. Meas. Technol. Conf.*, May 2008, pp. 985–990.
[6] M. Al Haek, *The Development of an Immune Inspired Energy Charging Mechanism for Swarm Robotic System* (Kulliyyah of Information and Communication Technology). Selangor, Malaysia: International Islamic University Malaysia, 2016.
[7] A. Couture-Beil and R. T. Vaughan, "Adaptive mobile charging stations for multi-robot systems," in *Proc. IEEE/RSJ Int. Conf. Intell. Robots Syst.*, Oct. 2009, pp. 1363–1368.
[8] W. Liu, K. T. Chau, C. H. T. Lee, C. Jiang, W. Han, and W. H. Lam, "Multi-frequency multi-power one-to-many wireless power transfer system," *IEEE Trans. Magn.*, vol. 55, no. 7, pp. 1–9, Jul. 2019.
[9] I.-J. Yoon and H. Ling, "Investigation of near-field wireless power transfer under multiple transmitters," *IEEE Antennas Wireless Propag. Lett.*, vol. 10, pp. 662–665, 2011.
[10] R. Johari, J. V. Krogmeier, and D. J. Love, "Analysis and practical considerations in implementing multiple transmitters for wireless power transfer via coupled magnetic resonance," *IEEE Trans. Ind. Electron.*, vol. 61, no. 4, pp. 1774–1783, Apr. 2014.
[11] Z. Yan, B. Yang, H. Liu, C. Chen, M. Waqas, R. Mai, and Z. He, "Efficiency improvement of wireless power transfer based on multitransmitter system," *IEEE Trans. Power Electron.*, vol. 35, no. 9, pp. 9011–9023, Sep. 2020.
[12] D. Arnitz and M. S. Reynolds, "Multitransmitter wireless power transfer optimization for backscatter RFID transponders," *IEEE Antennas Wireless Propag. Lett.*, vol. 12, pp. 849–852, 2013.

[13] M. Q. Nguyen, Y. Chou, D. Plesa, S. Rao, and J.-C. Chiao, "Multiple-inputs and multiple-outputs wireless power combining and delivering systems," *IEEE Trans. Power Electron.*, vol. 30, no. 11, pp. 6254–6263, Nov. 2015.
[14] L. J. Chen, W. I. S. Tong, B. Meyer, A. Abdolkhani, and A. P. Hu, "A contactless charging platform for swarm robots," in *Proc. 37th Annu. Conf. IEEE Ind. Electron. Soc. (IECON)*, Nov. 2011, pp. 4088–4093.
[15] S. Nikoletseas, Y. Yang, and A. Georgiadis, *Wireless Power Transfer Algorithms, Technologies and Applications in Ad Hoc Communication Networks*. Springer, 2016.
[16] M. Patil, T. Abukhalil, S. Patel, and T. Sobh, "UB robot swarm—Design, implementation, and power management," in *Proc. 12th IEEE Int. Conf. Control Autom. (ICCA)*, Jun. 2016, pp. 577–582.
[17] A. Sarin and A.-T. Avestruz, "Scaling wireless power transfer through code division multiple access," in *Proc. IEEE PELS Workshop Emerg. Technol., Wireless Power Transf. (Wow)*, Jun. 2018, pp. 1–6.
[18] A.-T. Avestruz, M. D. Rinehart, and S. B. Leeb, "Optimization of spread-spectrum MSK sequences and passive, multi-resonant bandpass rectifiers for wireless power transfer with low electromagnetic interference," in *Proc. IEEE 15th Workshop Control Modeling for Power Electron. (COMPEL)*, Jun. 2014, pp. 1–9.
[19] A. Sarin, X. Cui, and A.-T. Avestruz, "Comparison of switched receivers for direct-sequence spread-spectrum wireless power transfer," in *Proc. IEEE 18th Workshop Control Modeling Power Electron. (COMPEL)*, Jul. 2017, pp. 1–8.
[20] A. Sarin and A.-T. Avestruz, "Active segregated inductor for code division multiple access wireless power transfer," in *Proc. 20th Workshop Control Modeling Power Electron. (COMPEL)*, Jun. 2019, pp. 1–8.
[21] J. Wang, Z. Liang, and Z. Zhang, "Energy-encrypted contactless charging for swarm robots," in *Proc. IEEE Int. Magn. Conf. (INTERMAG)*, Apr. 2017, p. 1.
[22] L. Bayındır, "A review of swarm robotics tasks," *Neurocomputing*, vol. 172, pp. 292–321, Jan. 2016.
[23] E. Şahin, "Swarm robotics: From sources of inspiration to domains of application," in *Proc. Int. Workshop Swarm Robot.* Santa Monica, CA, USA: Springer, 2004, pp. 10–20.
[24] N. Eckenstein and M. Yim, "Design, principles, and testing of a latching modular robot connector," in *Proc. IEEE/RSJ Int. Conf. Intell. Robots Syst.*, Sep. 2014, pp. 2846–2851.
[25] L. Cheng, X. Ge, L. Hu, Y. Yao, W.-H. Ki, and C.-Y. Tsui, "A 40.68-MHz active rectifier with hybrid adaptive on/off delay-compensation scheme for biomedical implantable devices," *IEEE Trans. Circuits Syst. I, Reg. Papers*, vol. 67, no. 2, pp. 516–525, Feb. 2020.
[26] L. Shi, Z. Kabelac, D. Katabi, and D. Perreault, "Wireless power hotspot that charges all of your devices," in *Proc. 21st Annu. Int. Conf. Mobile Comput. Netw. (MobiCom)*, 2015, pp. 2–13.
[27] S. Li and C. Chris Mi, "Wireless power transfer for electric vehicle applications," *IEEE J. Emerg. Sel. Topics Power Electron.*, vol. 3, no. 1, pp. 4–17, Mar. 2015.
[28] J. G. Proakis and M. Salehi, *Digital Communications*, vol. 4. New York, NY, USA: McGraw-Hill, 2001.
[29] C. Jiang, K. T. Chau, T. W. Ching, C. Liu, and W. Han, "Time-division multiplexing wireless power transfer for separately excited DC motor drives," *IEEE Trans. Magn.*, vol. 53, no. 11, pp. 1–5, Nov. 2017.
[30] C. Zhao and D. Costinett, "GaN-based dual-mode wireless power transfer using multifrequency programmed pulse width modulation," *IEEE Trans. Ind. Electron.*, vol. 64, no. 11, pp. 9165–9176, Nov. 2017.
[31] Y. Zhang, Z. Zhao, and K. Chen, "Frequency decrease analysis of resonant wireless power transfer," *IEEE Trans. Power Electron.*, vol. 29, no. 3, pp. 1058–1063, Mar. 2014.
[32] R. W. Erickson and D. Maksimovic, *Fundamentals Power Electronics*. Cham, Switzerland: Springer, 2007.
[33] H. W. Alt, *Linear Functional Analysis: An Application Oriented Introduction*. London, U.K.: Springer-Verlag, 1992.
[34] A. Von Meier, *Electric Power Systems: A Conceptual Introduction*. Hoboken, NJ, USA: Wiley, 2006.
[35] J. Garnica, R. A. Chinga, and J. Lin, "Wireless power transmission: From far field to near field," *Proc. IEEE*, vol. 101, no. 6, pp. 1321–1331, Jun. 2013.
[36] H. Kobayashi, J. M. Hinrichs, and P. M. Asbeck, "Current-mode class-D power amplifiers for high-efficiency RF applications," *IEEE Trans. Microw. Theory Techn.*, vol. 49, no. 12, pp. 2480–2485, Dec. 2001.
[37] C. J. R. McCook and J. M. Esposito, "Flocking for heterogeneous robot swarms: A military convoy scenario," in *Proc. 39th Southeastern Symp. Syst. Theory*, Mar. 2007, pp. 26–31.
[38] A. Prorok, M. A. Hsieh, and V. Kumar, "The impact of diversity on optimal control policies for heterogeneous robot swarms," *IEEE Trans. Robot.*, vol. 33, no. 2, pp. 346–358, Apr. 2017.
[39] M. George, "BA scale-free network generation and visualization," *MATLAB Central*, vol. 12, Aug. 2006.

AKSHAY SARIN (Member, IEEE) received the B.Tech. degree in electrical engineering from IIT Roorkee, in 2013, and the M.S. degree in electrical engineering from the University of Michigan at Ann Arbor, in 2017, where he is currently pursuing the Ph.D. degree with the Department of Electrical Engineering and Computer Science. His research interests include modeling and control of power electronics.

AL-THADDEUS AVESTRUZ (Member, IEEE) received the S.B. degree in physics with electrical engineering, the S.M. degree in EE, and the Ph.D. degree in electrical engineering and computer science from the Massachusetts Institute of Technology, Cambridge, MA, USA, in 2006 and 2016. He is currently an Assistant Professor in electrical and computer engineering with the University of Michigan at Ann Arbor, MI, USA. He has over a decade of industry and entrepreneurial experience. He holds eight issued U.S. patents. His research interests include the design, modeling, and control of high-performance power electronics and wireless power transfer for energy, mobility, medicine, and the Internet of Things. His complementary research interests include circuits and systems for sensing, electromagnetic systems, feedback and controls, renewable energy, automotive, biomedical, and consumer applications. He was a recipient of the IEEE PELS Best ECCE Paper on Emerging Technology Award Oral Presentation, in 2019. He was the Associate Technical Program Chair of the IEEE Energy Conversion Congress and Exposition, in 2019. He is the Technical Program Co-Chair of the 2021 IEEE Wireless Power Week and the General Chair of the 24th IEEE Workshop on Control and Modeling for Power Electronics, in 2023. He is also an Associate Editor of the IEEE Open Journal of Power Electronics and a Guest Associate Editor of the IEEE Journal of Emerging and Selected Topics in Power Electronics.